ACTUATORS

Electrostatic bellow muscle actuators and energy harvesters that stack up

I. D. Sîrbu[1], G. Moretti[2], G. Bortolotti[1], M. Bolignari[1], S. Diré[1], L. Fambri[1], R. Vertechy[3], M. Fontana[1,2]*

Future robotic systems will be pervasive technologies operating autonomously in unknown spaces that are shared with humans. Such complex interactions make it compulsory for them to be lightweight, soft, and efficient in a way to guarantee safety, robustness, and long-term operation. Such a set of qualities can be achieved using soft multipurpose systems that combine, integrate, and commute between conventional electromechanical and fluidic drives, as well as harvest energy during inactive actuation phases for increased energy efficiency. Here, we present an electrostatic actuator made of thin films and liquid dielectrics combined with rigid polymeric stiffening elements to form a circular electrostatic bellow muscle (EBM) unit capable of out-of-plane contraction. These units are easy to manufacture and can be arranged in arrays and stacks, which can be used as a contractile artificial muscle, as a pump for fluid-driven soft robots, or as an energy harvester. As an artificial muscle, EBMs of 20 to 40 millimeters in diameter can exert forces of up to 6 newtons, lift loads over a hundred times their own weight, and reach contractions of over 40% with strain rates over 1200% per second, with a bandwidth over 10 hertz. As a pump driver, these EBMs produce flow rates of up to 0.63 liters per minute and maximum pressure head of 6 kilopascals, whereas as generator, they reach a conversion efficiency close to 20%. The compact shape, low cost, simple assembling procedure, high reliability, and large contractions make the EBM a promising technology for high-performance robotic systems.

INTRODUCTION

The development of electromechanical devices that are mechanically soft or compliant is expected to lead to robotic systems that can interact safely with humans and other living creatures (*1*). A key component of these robots is the actuation system, which is required to contribute to different motoric tasks, including soft joint motion/stretching, similar to mammalian muscles, or interaction with objects through inflatable/bendable interfaces (*2*, *3*).

In response to this need, the past decade has seen a huge effort to develop fluidic actuation systems (FASs) (*4*, *5*) and linear artificial muscles (AMs) (*6*–*8*) for soft robots. Robotic FASs are based on soft actuation structures capable of smooth interactions with the environment, but they require bulky compressors or pumps. Several works have been conducted to develop battery-based microcompressors (*4*) and lightweight fully polymeric pumps based on smart materials (*5*, *9*). The first have been successfully demonstrated in some robotic applications but have limited efficiency and scarce controllability, and they are inherently stiff and noisy. The latter rely on less conventional operating principles such as electroosmosis (*10*), thermo-pneumatic force (*11*), and charge-injection electrodynamics (*5*) and are suitable for very small–scale applications with flow rates below a few milliliters per minute, but they struggle to reach intermediate scales required for centimeter-scale robots.

In parallel, the past decade has also seen a huge effort to develop AMs able to produce displacements and forces in the ranges of 10^{-3} to 10^{-1} m and 10^{-3} to 10^{2} N, respectively. Traditional multipole electrical motors struggle to reach these scales because of the complexity in miniaturization, whereas microactuation systems (*12*) cannot be easily scaled up. Although thermally driven actuators (*13*, *14*) have been identified as promising options, their response is limited by slow heat transfer dynamics.

Electrostatic actuators are an interesting option for actuation of robots owing to their simple design (relatively small number of components), lightness, high efficiency, ease in control, self-sensing capabilities, and bidirectional operation (i.e., they can work as actuator and as generator in the passive phase of motion). Electrostatic actuators that take advantage of Maxwell pressures within an air gap are the most effective solutions in the length scale from 1 to 10 μm (i.e., for microelectromechanical systems) but do not effectively scale up in the millimeter to centimeter range due to the decrease of the dielectric strength in large air gaps. Dielectric elastomers (DEs) (*15*–*17*) have been introduced as a possible solution for electrostatic actuator upscaling. However, they require complex layouts with prestretched functional membranes (*18*), and their useful force is limited by the polymer mechanical stiffness.

In 2009, Najafi and coworkers (*19*, *20*) introduced the electrostatic hydraulic microactuator, which relies on a combination of deformable dielectrics and a dielectric liquid gap. Compared with microactuators with air gaps, these systems can bear larger electric fields. Compared with DEs, they present little or no force limitation due to the elastic stresses. The full potential of this concept was later proven at larger scales by Keplinger and colleagues (*21*) with the development of the HASEL (hydraulically amplified self-healing electrostatic) actuators. In parallel, Shea and coworkers (*22*) introduced the idea of zipping electrostatic actuators, i.e., a device in which two electrode-coated dielectric polymeric films come into contact through progressive increases in their contact surface, in response to an applied electric field. However, they obtained nonoptimal performance because of the use of air as the dielectric fluid. Later on, taking advantage of dielectric liquids, our group (*23*) demonstrated the possibility to revert the zipping actuation principle to perform electrical energy generation.

[1]Department of Industrial Engineering, University of Trento, Trento, Italy. [2]TeCIP Institute, Scuola Superiore Sant'Anna, Pisa, Italy. [3]Department of Industrial Engineering, University of Bologna, Bologna, Italy.
*Corresponding author. Email: marco.fontana@santannapisa.it

Among the most recent actuator concepts based on the zipping kinematics and a liquid dielectric, Peano-HASEL (*21*, *24*) and electro-ribbon AMs (*25*) demonstrated impressive results in terms of energy densities, on the order of 10^2 J/kg, despite the use of simple off-the-shelf low-cost materials such as polypropylene or other flexible polymeric films and dielectric oils. However, these devices were only demonstrated as AM actuators, and no proof of bidirectional actuator-generator operation was delivered.

Here, we present the electrostatic bellow muscle (EBM), a lightweight electrostatic transducer that combines fluid dielectrics, flexible electroactive films, and stiffening elements to form a deformable unit that contracts and pumps the dielectric fluid in response to an electrical stimulus. Unlike previously proposed concepts, an EBM device can alternatively work as: (i) a hydraulically coupled actuator (which exploits the fluid pressure to produce work on the external world), in the same fashion as HASELs (*21*); (ii) a purely electrostatic actuator (without pressurization of the dielectric liquid), in a similar fashion as electrostatic ribbons (*25*).

As contractile muscles, EBMs offer (i) suitability to be combined in arrays to achieve large strokes and forces and (ii) contractions over 40%, comparable with those of natural muscles and exceeding those of several AM technologies (*8*, *26*, *27*). As hydrostatic pump for FASs, EBMs outperform state-of-the art soft pumps based on dielectric polymers (*28*). Compared with Peano-HASELs, which excel in strain rate and power density but require external rolling/translating mechanisms (such as pulleys) to achieve actuation strains over 20% (*27*), EBMs provide larger contractions and better ease of stacking. Compared with electrostatic ribbons, which are capable of huge contractions of up to 100% (*25*), EBMs reach larger strain rates and provide more stable encapsulation of the dielectric fluid. In addition, EBM contractile muscles can operate in generation mode, converting pulsating mechanical energy into electricity, without modifications to their layout and loading mode, reaching an efficiency of about 20%. Therefore, they could be effectively used to implement power recycling during the passive/breaking phases of actuation.

As it stands, the EBM offers an alternative perspective to enable direct-drive actuation of soft lightweight robots that combine the AMs and FASs. Switching from actuator to generator mode might offer further opportunities to improve energy efficiency and produce a drastic reduction in the required battery capacity of autonomous robots.

RESULTS

EBM working principle

The EBM is an electrostatic transducer that converts electrical energy into mechanical work (or vice versa), taking advantage of electrostatic forces between oppositely charged electrodes (*29*), and it bears the ability to work both as an actuator and a generator (*16*, *24*, *30*, *23*). The EBM consists of a circular pouch made of two overlapped layers of compliant polymeric dielectric material holding opposite flexible electrodes on their external faces (Fig. 1, A to D). The dielectric layers are held together by annular frames attached along their perimeter. These frames have the role of maintaining the structural integrity of the EBM and constraining its deformation. The pouch has a single central opening on the top and contains a volume of dielectric liquid. The bottom of the pouch holds a rigid end effector for force application (Fig. 1B).

In the free state, the electrodes are flat, and the polymeric dielectric layers are in contact. Once a load is applied, the membranes deform out of plane, originating a liquid-filled pouch with a shape similar to a double-truncated cone shell.

In the actuation mode (Fig. 1C), with the application of a voltage, charges on opposite electrodes attract, causing the polymeric layers to be pulled toward each other in a "zipping" motion (*22*). During zipping, the polymeric layers gradually come into contact (starting from the perimeter), and liquid is evacuated through a central opening toward a reservoir.

Because of its layout, the EBM can pursue two different actuation modes: as a contractile actuator that does work against an external force or as a hydrodynamic actuator that does work against the pressure of the fluid. In the first mode, Maxwell stresses (*16*) are exploited to produce work against a force applied at the end effector, whereas the dielectric fluid is evacuated toward a soft-walled variable volume reservoir, hence resulting in little or no variation in pressure with respect to atmospheric conditions. In the second mode, Maxwell stress is used to induce a substantial pressurization in the fluid chamber, and the fluid is delivered to a fluid utility. In the generation mode, similar to DE generators (*31*), external mechanical forces drive the pouch deformation, whereas the voltage is properly varied in a such a way that electrical energy is generated and supplied to the driving electronics.

Modeling of EBM

The EBM can be modeled as a variable capacitor, using an approach similar to that presented in (*29*), introducing the following simplifications:

1) In a generic configuration, the EBM geometry can be ideally divided into two portions (Fig. 1D): a fully zipped outer region, in which two flat dielectric polymer portions face each other over an annular surface and a double-cone chamber in which the polymer layers enclose a volume of dielectric fluid. Further assumptions on the distribution of the strains in the dielectric polymer layers are discussed in the Supplementary Materials.

2) The electrical response is purely electrostatic; i.e., leakage currents through the dielectric layers are neglected. Similar to (*29*), the total capacitance of the device is about equal to that of the zipped annular portion, whereas the capacitance of the double-cone portion housing the oil is negligible.

The EBM kinematics is described through two independent parameters, i.e., the height h of the pouch and the radial distance r_c from the cone axis of the inner perimeter of the zipped region (Fig. 1D). The EBM response is governed by the following equations (see derivation and validation in the Supplementary Materials)

$$\begin{cases} F + p \cdot \dfrac{\partial \Omega_c}{\partial h} = \dfrac{\partial U_{el}}{\partial h} + \epsilon_p E^2 \cdot A_z \dfrac{\partial t}{\partial h} \\ p \cdot \dfrac{\partial \Omega_c}{\partial r_c} = \dfrac{\partial U_{el}}{\partial r_c} + \epsilon_p E^2 \cdot \left[2\pi t r_c + A_z \dfrac{\partial t}{\partial r_c} \right] \end{cases} \quad (1)$$

where r_o and r_i are the fixed inner and outer radii of the device; $\Omega_c = \pi h(r_i^2 + r_c + r_i r_c)/3$ is the volume of fluid in the double-cone chamber; $U_{el} = U_{el}(h, r_c)$ is the elastic energy of the deformed polymer layers; $A_z = \pi(r_o^2 - r_c^2)$ is the area of the zipped electrode portion; $t = t(h, r_c)$ is the thickness of a single polymer layer in the zipped region (it varies with h and r_c due to strain); ϵ_p is the dielectric constant of the polymer; and E is the electric field in the zipped region, which depends on the applied voltage V: $E = V/(2t)$. The two

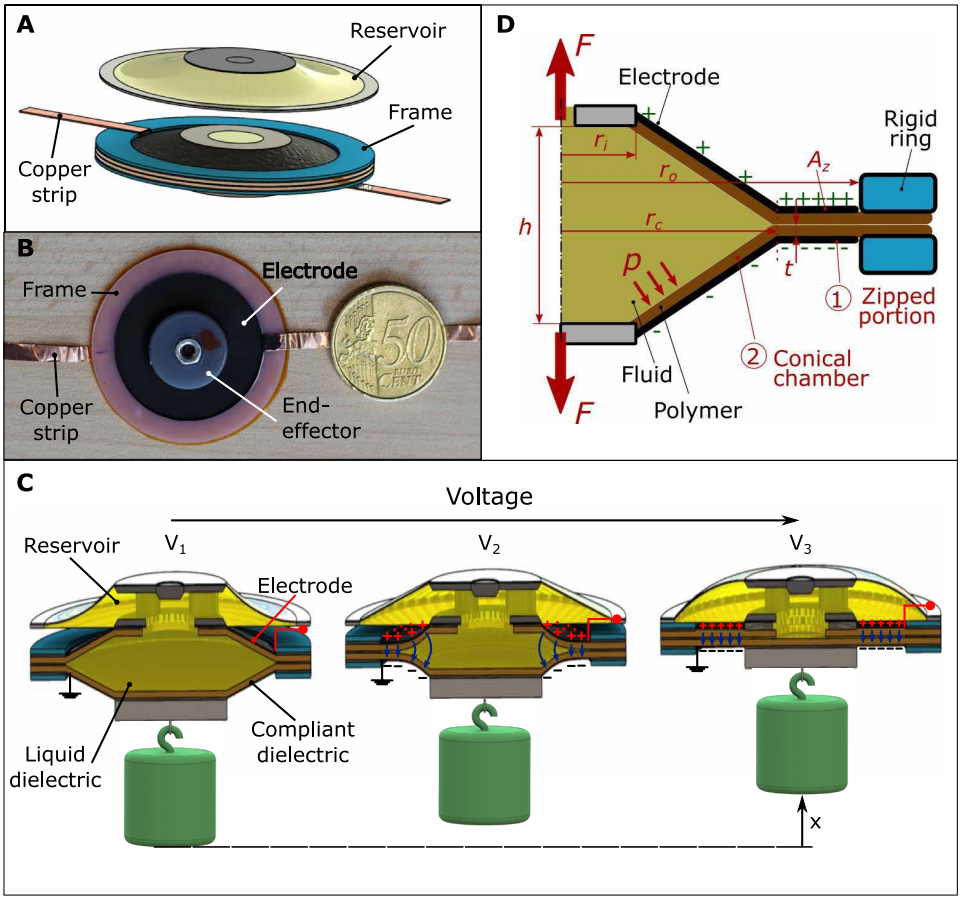

Fig. 1. Design and working principle of the EBM. (**A**) Representation of the EBM. (**B**) Photograph of an EBM prototype (bottom view) with reinforcing rings. The diameter of the coin, introduced for comparison, is 24.25 mm. (**C**) Schematic of the EBM with integrated fluidic reservoir and phases of the actuation at three different voltages ($V_1 < V_2 < V_3$). In the initial state, the pouch is completely open under the action of a load. At the intermediate voltage, zipping takes place, and the load is pulled up. At the maximum voltage, the device is fully zipped, and the liquid dielectric between the polymer layers is minimum. Blue arrows in the picture qualitatively represent electric field streamlines. (**D**) Modeling of an EBM with inner and outer radii r_i and r_o as a combination of two portions: a flat zipped portion with thickness t and area A and a conical fluid chamber with radius r_c and height h. An external force F and an internal fluid pressure p are applied on the EBM.

terms on the righthand side of both equations in Eq. 1 account for the elastic restoring forces due to the dielectric polymer elasticity and the contribution of Coulomb electrostatic forces. The latter contribution, in particular, holds a term $\epsilon_p E^2$ proportional to the Maxwell stress applied on the polymeric layers over the zipping region.

The response of the EBM in the different working modes can be described in terms of the different applied loads (namely, F or p in Eq. 1). When the EBM works as a contractile actuator, the fluid dwells at a pressure close to atmospheric value ($p \simeq 0$), and the force F, which makes work in the direction of h, represents the useful output load. When the EBM works as a pump, p represents the useful available pressure, and F is either zero or equal to a constant preload. As a generator, the EBM can take advantage of either the input mechanical work provided by the external force (reverse muscle) or by the fluid pressure (reverse pump) to produce an electrical energy output.

Manufacturing EBMs

The pouch consists of two layers of dielectric polymer attached together with a thin annular layer of double-sided adhesive film. The top film has a circular opening serving as the fluid outlet. Stiff reinforcing annular frames are bonded on the outer faces of the dielectric films with the aim of preventing deformations at the outer diameter of the films. A reservoir is connected to the top opening and an end effector on the bottom side (Fig. 2A). The reservoir includes a manifold that generates a radial fluid flow from the axial movement of the EBM and a slack membrane that implements a (nearly) constant-pressure variable-volume sealed reservoir. Conductive paint is applied on each side of the pouch (Fig. 2B) to form the electrodes. The device is preloaded and filled up with dielectric oil through the central opening (Fig. 2C).

EBM operated as a contractile actuator

An EBM unit can work as a contractile actuator achieving contractions of up to 20% its initial length (including the length of the fluid reservoir) against external loads in the range from 1 to 6 N (up to roughly 70 times the whole muscle and fluid storage weight) with input voltages in the range from 6 to 8 kV. At 1 Hz, the EBM unit produced strokes of 1.3 mm (Fig. 3A) corresponding to a contraction of 18.0% of the length before actuation, with a maximum applied voltage of 6 kV. Neglecting the contribution of the reservoir height, the stroke corresponds to a contraction of 44.7%. Figure 3A reveals that at 1 Hz, the device sweeps the whole available stroke and remains latched at the upper and lower positions for a finite amount of time. The EBM moves synchronously with the applied voltage: When voltage is low, concurrent polymeric layers are kept apart (unzipped) under the action of the mechanical load; as the voltage increases, electrostatic forces progressively overcome the external load and cause the electrodes to zip; at large voltage (roughly above 5 kV), the electrodes stay fully zipped against each other, and almost all of the liquid is moved into the reservoir. The EBM experiences a very limited reduction in stroke due to increased frequency (Fig. 3A), similarly to hydraulically amplified muscles (*24*) and in contrast with frequency-sensitive fluid-based electrostatic ribbons (*25*). The EBM stroke at 4 and 8 Hz is, respectively, 97.0 and 92.8% of the stroke at 1 Hz, with a load of 1.5 N. Increasing the peak voltage to 8 kV, the EBM reaches a total contraction over 20% with forces of up to 2 N. An overview of the EBM unit response under quasi-static conditions under different applied forces is shown in Fig. 3B. In the low-force range (1 to 2 N), increasing the applied load leads to an increase in the stroke as a result of the increased initial length of the muscle. A further increase in the load, which acts against the electrostatic forces, causes a decrease in the actual stroke. The EBM still generates contractions over 17%

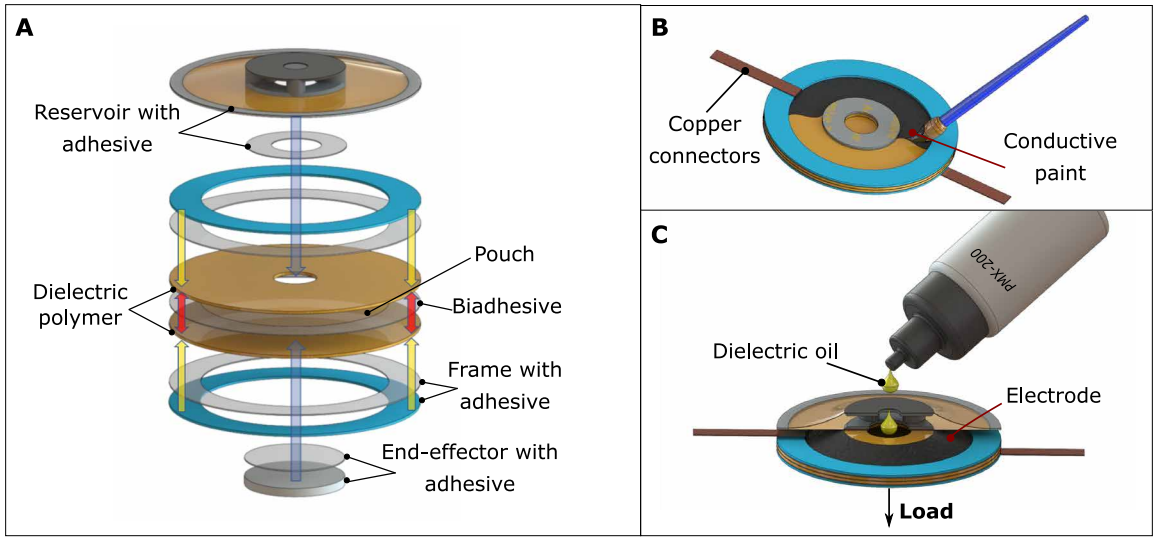

Fig. 2. Layout and fabrication procedure of an EBM unit. (**A**) Exploded view of the EBM. Red arrows show the bonding of two dielectric layers with a thin adhesive on a circular edge. Blue arrows show the bonding of structural annular frames on the two sides of the pouch. Yellow arrows represent the application of the end effector and the fluid reservoir. (**B**) Electrodes are painted on the external surfaces of the dielectric layers with conductive paint. Flexible copper-tape connectors are used to create the connection with the circuit wires. (**C**) The EBM is filled with dielectric oil through an opening in the reservoir. The opening is sealed after filling.

with loads of up to 3 N—i.e., an equivalent lifting capability of 35 times its total weight (including the weight of the fluid reservoir) and 50 times the EBM core weight. Increasing the peak voltage generates a modest increase in stroke at small loads, whereas it has a relevant impact at high loads. In effect, at reduced loads, a relatively low voltage is sufficient to cause a contraction close or equal to the whole geometrically available stroke. A larger voltage still produces larger strokes even at 1 to 1.5 N, because it enables better fluid evacuation and the permanence of a thinner trapped fluid film in the fully zipped configuration.

In the range from 1 to 10 Hz, the EBM contraction weakly depends on the frequency even at relatively large applied loads (Fig. 3C). At 2.5 N, the contraction is nearly constant (close to 19%) at 8 kV in the range from 1 to 10 Hz, whereas it slightly decreases with frequency at 6 kV (with the stroke at 10 Hz still being 74.6% that at 1 Hz), because the electrostatic forces do not completely compensate viscous and hydraulic losses. The EBM provides actuation up to frequencies of at least 80 Hz (Fig. 3C) with 2 N of applied load, experimenting a reduction in stroke of 50% at a frequency of 37 Hz and of 80% at 80 Hz. The reduction in stroke at larger frequencies is ascribable to viscous losses due to the dielectric fluid motion.

The blocking force of the EBM (at which the stroke falls to zero) at 8 kV is close to 6 N (i.e., 98 times the weight of the EBM core), rather independently of the actuation frequency (Fig. 3D). The stroke at 5 N is roughly 65% of the maximum stroke, and it drastically falls in the interval of 5 to 6 N. The EBM unit achieves contraction rates of up to 1140%/s at 10 Hz (fig. S8), with power densities over 21 W/kg per EBM core mass (which still corresponds to 14.8 W/kg if the weight of the fluid reservoir is also considered).

The EBM has also achieved notable performance in terms of long-term cyclic operation. An EBM prototype subject to electric fields in the order of 120 kV/mm on the dielectric polymer layers was able to accomplish more than 0.1 millions of cycles at a 5 Hz operating frequency, with no visible reduction in stroke over time (fig. S11).

Scaling the EBM response

We investigated the effect of scaling the radial dimensions of an EBM contractile actuator while keeping the thickness of the dielectric polymer layers constant. According to the proposed mathematical model, a geometrically scaled device (with geometric scaling factor of s_f) loaded with a force scaled by s_f provides a stroke that is s_f times larger at a same voltage (derivation provided in section SA.3).

The experimental data on three different devices (i.e., the base-case device to which previous results refer, a smaller scale device with $s_f = 2/3$, and a larger device with $s_f = 4/3$) confirm the trends predicted by the model (Fig. 3E and fig. S9). Observed disagreements are possibly due to the reduction in stiffness of the structural rings for the upscaled device and a higher sensitivity to imperfect manual manufacturing of the downscaled device.

Reducing the scale of an actuator leads to an increase in the achievable energy density (see section SA.3 in the Supplementary Materials) due to the substantial reduction in the dielectric fluid mass (which scales with s_f^3, as opposed to the actuation work, which scales with s_f^2). A downscaled EBM prototype with lightweight polymeric structural components was able to achieve an energy density (i.e., cyclic actuation work per unit EBM core mass) of 1.16 J/kg subject to a load of 1.6 N, i.e., 127 times its own weight (fig. S10).

EBM arrays from foldable strips for scaling up force and stroke

EBM units can be combined in series and in parallel to magnify the stroke and the force, respectively, while preserving the ease of manufacturing and assembly of single-unit AMs. In-series connection is achieved by stacking up multiple devices (*32*, *33*) and putting their fluid chambers in communication. In-parallel connection is achieved by providing a set of EBM units/stacks with a common end effector. By connecting in parallel m stacks of n in-series EBMs, we obtain $m \times n$ arrays that provide a stroke that is n times magnified in the presence of an applied force that is m times as much.

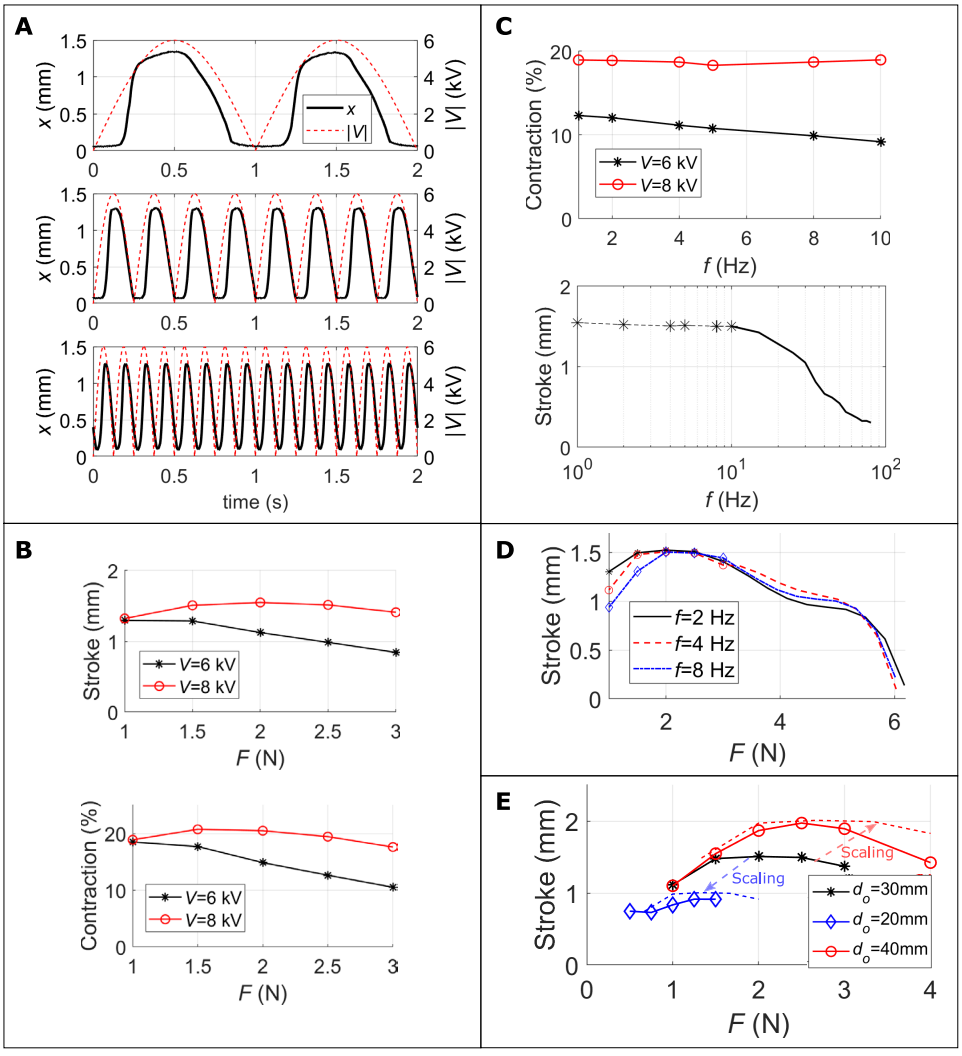

Fig. 3. Force-contraction response of an EBM unit. (**A**) Time series of the voltage V and actuator displacement x at 1 Hz (top), 4 Hz (middle), and 8 Hz (bottom) with a load of 1.5 N. The voltage modulus is shown for clarity, although in practice, its polarity is reverted at each cycle. (**B**) Force-stroke (top) and force-contraction responses at 1 Hz (bottom), with different applied forces F and voltages. (**C**) Frequency response at different voltages, with a 2.5-N load (top). Markers refer to tests with different voltage. Results of maximum-frequency test with a 2-N load and 8-kV voltage (bottom). The dashed line with markers refers to constant-frequency tests, whereas the continuous line refers to a test with chirp voltage input. (**D**) Blocking force test at different frequencies f with a voltage of 8 kV. Markers refer to constant force, whereas line extensions refer to tests with progressively increasing force. (**E**) Force-stroke response of three different EBMs: the base-case device (outer diameter d_o = 30 mm) and two versions with radial dimensions scaled by a factor s_f = 2/3 (d_o = 20 mm) and s_f = 4/3 (d_o = 40 mm), respectively. Markers represent constant-force constant-frequency measurements (4 Hz, 8 kV), whereas dashed lines represent theoretically scaled responses with respect to the base-case scenario.

Different array layouts can be built through the same manufacturing procedure (Fig. 4, A to D, and fig. S4). The constitutive elements of the EBM units (electrodes, central openings, and frames with adhesives) are mounted equidistantly and collinearly on a strip of dielectric material, forming a row of "half-units" on one surface of the strip. Figure 4A shows such a strip in the case of a four-unit array. This strip is then folded in half (with the frames and the electrodes on the external faces) to create EBM units (Fig. 4B). In the same way as single EBM units, each couple of half-units is attached and sealed together with thin layers of double-sided adhesive film. The resulting strip of assembled single units can be folded again to create arrays with arbitrary size. Figure 4C shows folds required to create a 2 × 2 EBM array, where a strip with two units is folded onto another one of the same size. In Fig. 4D, the same initial strip is folded in a different way so as to create a 1 × 4 array.

Starting from a strip of p EBM units, arrays of different sizes can be created, obtaining a maximum blocking force equal to p times that of the single units (in the case of a $p \times 1$ array) or a maximum stroke equal to p times that of a unit (in the case of a $1 \times p$ array). To create an $m \times n$ array from a strip of p units (with $p = m \cdot n$), $n - 1$ folds are required. The simplicity of this assembly procedure makes it scalable and well suitable for mass production.

Performance of contractile EBM arrays

We built EBM arrays with different configurations, comprising up to six pouches each (Fig. 5A), with the same reference dimensions for the units as those used in Fig. 3 (A to D). By connecting six in-series EBM pouches (Fig. 5B) in a 1 × 6 arrangement, we reached strokes of up to 43% the muscle initial length (including the height of the fluid reservoir). We characterized the response of in-series arrays with loads of up to 3 N (20 to 40 times their weight). We compared the performance of 1 × 3 and 1 × 6 arrays against that of a single-unit device (Fig. 5C): At 8 kV, the stroke against a force of 1.5 N surpassed 4.1 mm for a 1 × 3 device (31.0% contraction) and 9.0 mm for a 1 × 6 array (42.8% contraction), as compared with 1.5 mm for the single-unit device (20.2% contraction). By increasing the number of in-series units, the height of the fluid reservoir (which is the same for all devices) becomes increasingly small compared with the total stroke, leading to an increase in the percentage contraction. Reducing the fluid reservoir height would generate an increase between 10 and 30% in the contraction for the different arrays. For instance, at 1 N, the estimated contraction for the 1 × 6 EBM would rise to 55.2% (as compared with 43.3%) if the reservoir height was virtually reduced to zero.

We compared the dynamic responses of different in-series EBM units (Fig. 5D and movie S1). Similar to the unit actuator, in the range from 1 to 10 Hz, the contraction achieved by EBM arrays is weakly dependent on the frequency. Compared with single and 1 × 3 devices, the 1 × 6 arrays suffer larger reductions in contraction

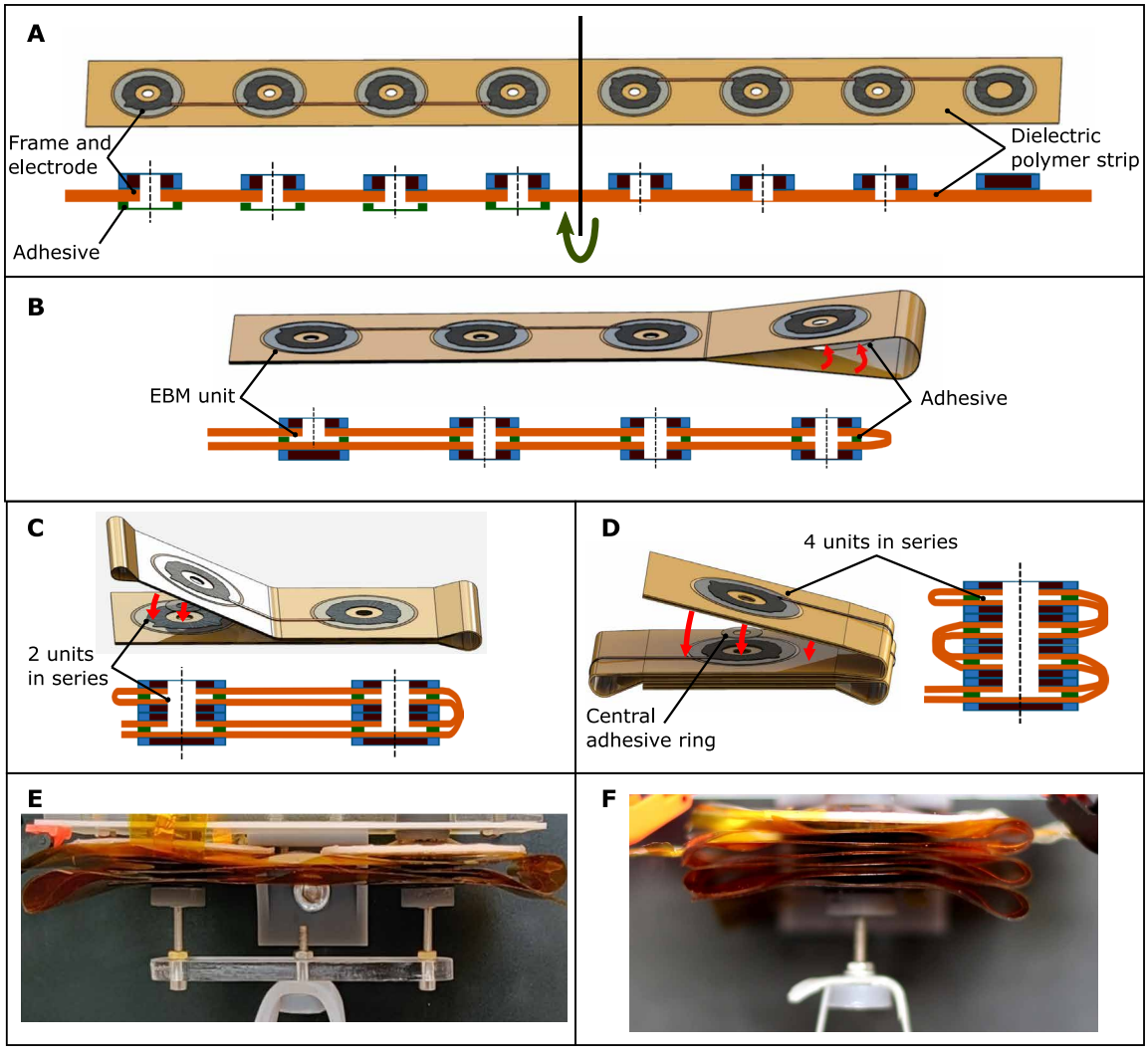

Fig. 4. Folding procedure of dielectric polymer strips to fabricate EBM arrays. (**A**) Dielectric polymer strip with frames, electrodes, and adhesive tape attached, represented both in 3D and cross-sectional view. The black vertical line represents the first fold. (**B**) 3D and cross-sectional views of the four parallel units created by the folding procedure. (**C**) 3D and cross-sectional views of a 2 × 2 EBM array obtained by folding. In-series units are attached together around the perimeter of their adjacent openings with annular-shaped double-sided adhesive film. (**D**) 3D and cross-sectional views of a 1 × 4 EBM array obtained by folding. (**E**) Photograph of a 2 × 3 EBM array. (**F**) Photograph of a 1 × 6 EBM array.

at large frequencies (above 5 Hz). This is due to dynamical effects (e.g., the increase in inertia with the number of units) and the higher sensitivity to manufacturing/misalignment errors of large EBM arrays.

EBM arrays of in-series units were able to reach peak linear speeds close to 200 mm/s (see fig. S13) and contraction over 1250%/s (see fig. S12). We measured a peak-specific power of 31 W/kg (see fig. S12) for the 1 × 3 actuator in the same order as other fluid-based electrostatic actuators (*24*, *25*). Shape-memory alloys and coiled nylon AMs reach higher power densities of tens of watts per gram (*14*, *34*). Nonetheless, they suffer from poor controllability at large frequencies (*24*) due to their slow thermal dynamics.

We developed a 2 × 3 EBM array made of two in-parallel 1 × 3 arrays (Fig. 4E). As expected, this device produces a stroke close to that of a 1 × 3 array in the presence of a load that is twice as much (Fig. 5E, fig. S14, and movie S2). In practice, scaling the force-stroke response of a 1 × 3 EBM array by a factor of 2 along the force axis leads to a slight overestimation of the 2 × 3 array stroke. This is due to a higher sensitivity of the 2 × 3 device to bending moments generated by the total load, applied between (and roughly parallel to) the axes of the in-parallel stacks. We used the 2 × 3 EBM array to lift large weights (see movie S2). The device can lift hanged masses as high as 1000 g, i.e., over 40 times its weight. This is consistent with the results of single-unit devices (Fig. 3D), which showed blocking forces for single units (and, virtually, in-series arrays) close to 6 N.

EBM for volumetric pumping

EBM arrays can be used as volumetric pumps capable to operate FASs. We used a 1 × 6 EBM with reference dimensions to inflate a thin elastomeric membrane with a 45-mm base diameter, and we reached operating pressures of up to 6 kPa and flow rates over 0.5 standard liters per minute (SLPM).

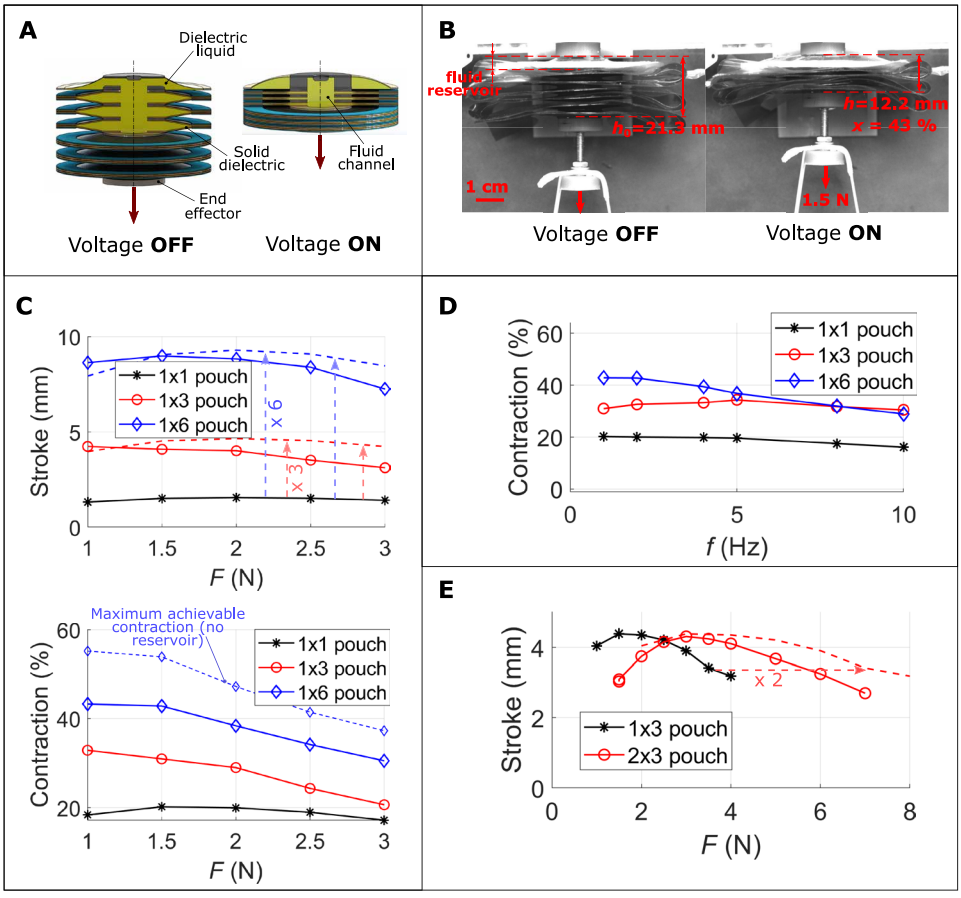

Fig. 5. Performance of arrays of EBM units. (**A**) Schematic of a 1 × 6 array. (**B**) A 1 × 6 array subject to a voltage of 8 kV produces a stroke *x* of 43% against a 1.5-N load at 1 Hz; h_0 and *h* denote the EBM length before and after contraction, respectively. (**C**) Comparison of the quasi-static force-stroke response of 1 × 1,1 × 3, and 1 × 6 EBM arrays subject to 8-kV actuation cycles at 1 Hz. The top plot compares the absolute strokes, whereas the bottom one reports the percentage contraction. Dashed lines in the top plot represent the stroke of a unit pouch multiplied by 3 or 6, as compared with the stroke of the arrays. The dashed line in the bottom plot represents the achievable contraction in case the fluid reservoir height was reduced to zero. (**D**) Frequency response of 1 × 1,1 × 3, and 1 × 6 arrays subject to 1.5 N and 8 kV. (**E**) Comparison of the response of 1 × 3 and 2 × 3 EBM arrays subject to 8-kV actuation at 4 Hz. The dashed line represents the response of the 1 × 3 device scaled by 2 along the force axis, as compared with the response of the 2 × 3 device.

The EBM-based volumetric pump was obtained by putting the dielectric liquid chamber in communication with the air chamber that holds the membrane and using two check valves to produce a unidirectional flow (Fig. 6A), similarly to (*28*). With this layout, each stroke of the dielectric liquid free surface generates a useful unidirectional air flow from the atmosphere toward the bubble. By performing tests at 7 Hz with a voltage of 8 kV and a preload of 1.5 N, we were able to inflate the balloon up to 56 cm^3 in 28 s (Fig. 6B and movie S3). By performing tests at different frequencies, we observed that the pumped volume increases nearly proportionally with the frequency. The trend of the pumped volume and pressure versus the number of actuation cycles is about the same at operating frequencies of 5 and 7 Hz (Fig. 6B). However, at low frequency (i.e., 3 Hz), the pressure and air volume delivered after a same number of cycles are lower. This is possibly due to air leaks in the pump body, which are independent of the pumping frequency and are not counterbalanced by a sufficient delivered flow at low operating frequencies. The pump flow rate (averaged on the single actuation cycles) as a function of the hydrostatic pressure has the trend shown in Fig. 6C. In the low-pressure range (below 2 kPa), the EBM pump delivers a flow in the range of 0.40 to 0.63 SLPM, which increases with the frequency. Under these conditions, the EBM sweeps a stroke close to 5 mm (corresponding to a volumetric displacement of 2.1 cm^3) and delivers a nearly constant volumetric displacement. By measuring the bubble volume variation within a cycle (see lens in Fig. 6B), we estimated a maximum instantaneous flow rate of 1.95 SLPM (fig. S17B). As the hydrostatic pressure increases, the EBM stroke and hence the flow rate decrease. As expected, at given pressure, the delivered flow rate increases with the actuation frequency following a nearly linear trend (Fig. 6D). The blocking pressure, above which the pump is no longer able to supply a flow, is slightly larger than 6 kPa, both at 5 and 7 Hz. At lower actuation frequency, the blocking pressure decreases due to air leaks (Fig. 6C). At the blocking pressure, the EBM still exhibits a stroke of 2 mm, even though the supplied flow is equal to zero. This is due to air leaks and the effect of air compressibility in the pump body. The EBM was able to develop a pumping power (cycle average) of up to 18 mW (corresponding to a power density over 0.9 W/kg per unit EBM core mass) and instantaneous peak values of 68 mW (fig. S17).

The performance achieved by the EBM pump is comparable to that of the best-performing smart material–based FASs with similar dimensions. Similar figures of merit have only been achieved by state-of-the-art DE-driven pumps, exploiting snap-through instability of inflatable membranes (*35*) or a dynamic resonant design (*28*, *36*). Compared with the first solution (*35*), the EBM pump offers the potential for more compact designs. Compared with resonant DE FAS (*28*), the EBM pump achieves large flow rates with lower actuation frequency (below 10 Hz) and with no stringent need to tune the operating frequency. At a reference pressure of 2 kPa, our prototype generated a flow rate on the same order as that of a DE pump with similar radial dimensions (*36*) but with frequencies one order of magnitude lower.

EBM for energy harvesting

EBM arrays can function as generators with no need for architectural modifications compared with the actuator embodiment. To demonstrate generator operation, we supplied mechanical energy to a lightweight 1 × 3 EBM with polymeric structural rings by connecting the end effector to the slider of a linear motor via a pulling nylon cable, and we controlled the applied voltage synchronously with the

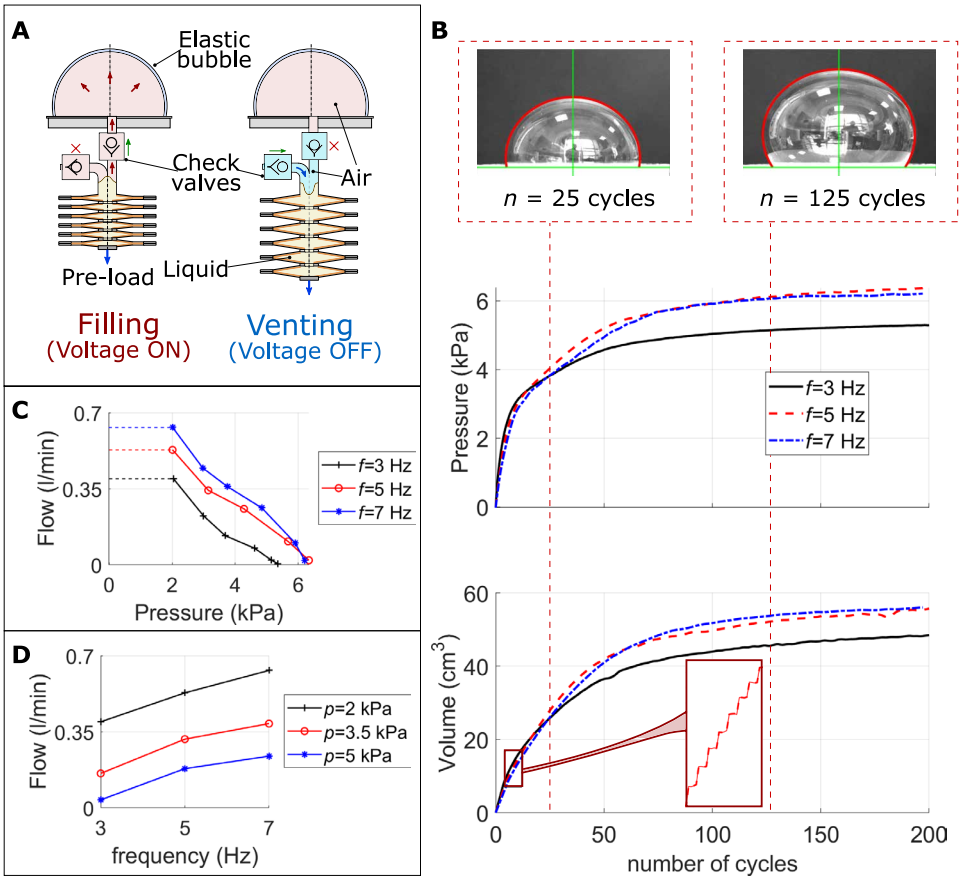

Fig. 6. Characterization of an EBM for volumetric pumping. (**A**) Operating principle of the EBM-driven pump. The EBM output is connected to an air chamber holding two check valves. The dielectric liquid free surface acts as the pumping element. Working cycles consist of a venting phase and a filling phase through which air is unidirectionally transferred from the atmosphere to the air chamber. (**B**) Trends of the pressure and the pumped volume as a function of the number *n* of pumping cycles at different frequencies *f* (3, 5, and 7 Hz). The top boxes show the progression of the balloon expansion, whereas the lens shows the stepwise volume increase for the test at 5 Hz (each step corresponds to a single stroke of the EBM). (**C**) Pressure-flow diagram of the EBM pump at different frequencies. The pressure increases from 0 to 2 kPa only span a few actuation cycles; therefore, the trend of the flow over the interval of 0 to 2 kPa is replaced with its average value (dashed lines). (**D**) Flow rate as a function of the frequency at three different pressures *p*.

motor displacement. We applied a constant voltage while the motor was pulling the EBM's end effector downward (pushing the electrodes apart) and kept the device uncharged while the motor was moving upward (allowing the electrodes to move closer) (Fig. 7A). By doing so, an amount of electrical energy is initially spent when voltage is applied; then, as the external mechanical load forces opposite electrodes to be pushed apart, the EBM positively delivers current, leading to a net gain of electrical energy. The electrical energy balance is depicted in Fig. 7B, which relates the EBM voltage to the total charge delivered by the power supply (*30*). Figure 7C shows the EBM force against the end-effector position: Because of voltage application, the force required to pull the electrodes apart (forward stroke) is larger than that required to allow the fluid discharge (return stroke), i.e., a net amount of mechanical work is supplied to the EBM at each cycle. Using different values for the priming voltage, we obtained a cyclic generated energy density of up to 0.41 J/kg (per EBM core mass), average power of up to 1.5 mW, and maximum efficiency close to 20% (Fig. 7D). The peak power output (for the test in Fig. 7A) is 80 mW, corresponding to a peak power density of 11.2 mW/g. These figures of merit increase monotonically with the priming voltage. In contrast with theoretical trends for electrostatic generators (*30*), the power and energy density have a subquadratic trend, possibly due to an increase in the leakage currents with the voltage.

As compared with DE generators, the stored elastic energy (due to mechanical loading) for EBMs is on the same order as the maximum stored electrostatic energy, whereas in DE generators, it is 3 to 50 times the stored electrical energy (*37*). This is a distinguishing feature that makes it easier coupling EBM harvesters with mechanical energy sources without the need of stiffness cancellation mechanisms (e.g., negative springs) (*38*, *39*).

The values of energy and power densities could be largely improved to get closer to the values achieved by DE generators [i.e., energy densities on the order of hundreds of joules per kilogram and power densities on the order of hundreds of watts per kilogram (*40*, *41*)]. Because of the low elastic energy stored in EBMs, mechanical losses are lower than in DE generators; nonetheless, charge leakages are estimated to be substantial. Figure 7B shows that the charge absorbed by the EBM (which differs from the real charge on the electrodes due to leaks) is notably larger than zero by the end of the cycle (state P_4), meaning that some current has been drained. These losses appear attributable to leaks in air (because the outer surfaces of the electrodes are not shielded) and through the dielectric layers, with the former likely being more relevant. Introducing shielding of electrodes and using different dielectric liquids might be the key to enhance EBM generator performance. In addition, optimizing the applied voltage waveform (*40*) and the duration of the charging/discharging phases and resorting to closed-loop logics is expected to lead to further improvement.

DISCUSSION

Here, we introduce a class of easy-to-manufacture actuators, called EBMs, that hold the ability of implementing different operating modes through a single device layout. Besides working as linear actuators that contract on activation, EBMs can also operate as hydrostatic pump for fluidic actuators or as energy harvesters. For each of these modes, they show performance that is comparable to that of other promising single-purpose electrostatic actuators (*21*, *24*, *25*). Straightforward magnification of EBM displacements and forces can be obtained through stacking and parallelization of units with a simple folding process, which is promising for mass production.

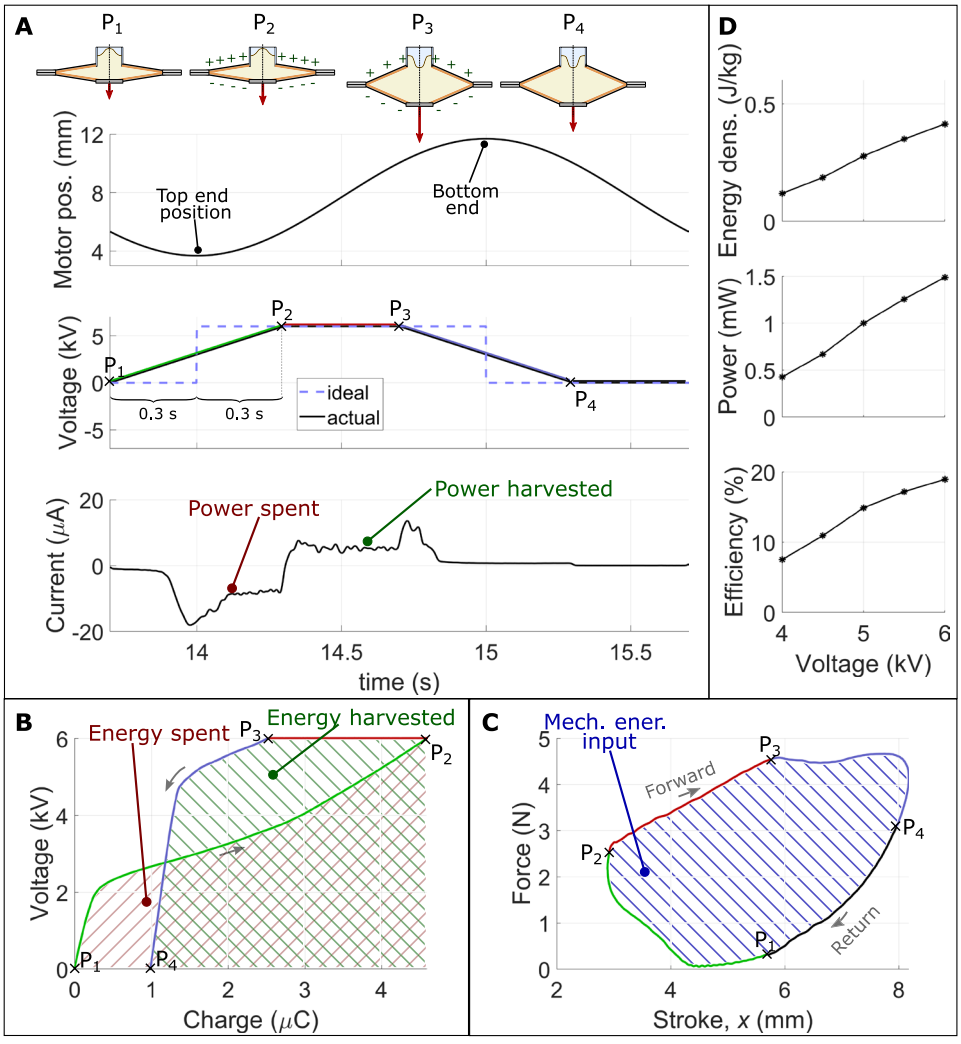

Fig. 7. Characterization of an EBM energy harvester. (**A**) Time series illustrating the working cycle of the EBM generator throughout configurations P1 to P4. Top: Input motor position (positive values represent downward displacement with respect to the EBM fully zipped configuration). Middle: EBM voltage (here, maximum voltage is 6 kV). Bottom: Output current of the EBM. Ideally, the generator is held at constant voltage while the stroke increases and uncharged while the stroke decreases (dashed curve). In practice, charging (discharging) is started 0.3 s before and concluded 0.3 s after the motor has reached the top (bottom) end of its stroke, to limit currents and losses. (**B**) Applied voltage versus supplied charge trajectory and (**C**) force versus end-effector stroke trajectory for the test of the previous sub-figure (the stroke x is equal to zero when the EBM units are flat). The hatched areas in the voltage-charge plane represent the electrical energy spent for priming and that positively supplied by the generator. The hatched area on the force-stroke plane equals the input mechanical energy. (**D**) Generated energy density, mean power, and mechanical-to-electrical efficiency as a function of the applied voltage.

As contractile actuators, EBM arrays reach contractions of up to 43%, i.e., more than two times the typical contractions of skeletal muscles (*8*). EBM AMs reach performance on the same order as other recently developed fluid-based electrostatic actuators. Compared with Peano-HASEL actuators, the EBM reaches larger contractions, with a moderately lower power density (*24*, *27*). Compared with electro-ribbons, EBMs reach smaller contractions but a substantially larger strain rate, while guaranteeing a tighter encapsulation of the dielectric fluid (*25*). As hydrostatic drivers for FASs, centimeter-scale EBMs can generate pressures of a few kilopascals [comparable or better than other smart material–driven pump prototypes (*5*, *36*)] and flow rates on the order of ~1 SLPM [larger than those of existing smart material–based pump prototypes and on the same order as commercial microcompressors (*4*)]. As energy harvesters, thanks to their high generated-to-elastic energy ratio, they can generate electrical power with efficiencies of up to 20%.

The EBM could be promising for robotic systems due to its lightness, scalability, and adaptability to different tasks. The added ability to harvest energy could also be an advantageous feature for autonomous battery-powered robots (*42*). In the future, the use of high-permittivity, high-strength dielectric polymers and the miniaturization of EBM units might improve power and energy densities and reduce required operating voltages. In generation mode, the use of fluids with better dielectric properties and an improved encapsulation of the electrodes seem key factors to further improve efficiency.

MATERIALS AND METHODS

EBM materials and components

The dielectric layers in EBM are made of 25-μm-thick LINQTAPE PIT1N polyimide (PI) film by Caplinq, with nominal relative permittivity of 3.9 and dielectric strength of 236 kV/mm (*43*). The dielectric fluid is Xiameter PMX 200 50 cSt, a silicone oil with a relative permittivity of 2.7 (*23*).

Bonding of the dielectric layers on the pouch inner surfaces is made with 5-μm double-sided adhesive tape by Nitto (no. 5600). Rigid rings are attached to the dielectric layer via 100-μm-thick double-sided adhesive tape by Tesa (68144). We produced two different versions of the EBM on the basis of different materials for the structural rings: a version with thin rigid metallic frames (to grant a reduced initial length and hence achieve larger contractions) and one with lightweight PMMA (polymethyl methacrylate) rings (to reduce the weight and increase the energy density). Metallic annular frames made of steel, with a thickness of 0.1 mm, were used for the actuator and pump tests. PMMA polymeric frames with 0.5 mm thickness were used for generator tests, although some actuation tests were also performed on PMMA-based EBMs (fig. S10).

Electrodes (16 mm by 30 mm in the base-case device) are made of DAG-T-502 carbon paint by Ted Pella. This paint shows appropriate compliance and adhesion to the substrate. To attach pouches in-series in arrays and to attach the reservoir or the end effector, we used 0.5-mm-thick 3M VHB 4905 double-sided adhesive tape.

The fluid reservoir contains three main components: a rigid layer, a manifold (which controls the direction of the flow within the reservoir), and a flexible membrane. The rigid layer consists of a PI film reinforced by a 0.5-mm-thick PMMA annular frame. The manifold is printed with a Formlabs 3D printer with Grey Pro photopolymer resin. The flexible membrane is a loosely stretched layer of 3M VHB 4905, which grants the reservoir with variable volume while producing negligible pressurization in the fluid. The total height of the reservoir is 4.3 mm, whereas its mass is 2.6 g.

EBM prototypes with different radial sizes were built. A base-case reference set of dimensions were used for most of the reported tests (Figs. 3, A to D, and 5 to 7). The reference EBM has outer electrode diameter d_o = 30 mm and was realized with either 30 mm–by–42 mm steel rings (Figs. 3, A to D, 5, and 6) or 30 mm–by–40 mm PMMA rings (Fig. 7). A complete set of reference dimensions for EBM unit prototypes are summarized in Fig. 2A, fig. S5, and table S3. Smaller- or larger-scale prototypes with thin steel rings (20 mm by 32 mm and 40 mm by 52 mm) or PMMA rings (20 mm by 27 mm) were also realized to study the scaled response of AM EBMs (Fig. 3E). The dimensions and weights of the different prototypes used for the tests are summarized in table S3.

Testing methods

A test bench was developed and adapted to characterize EBMs (unit and stacks) in different working modes (see fig. S6). High voltage was supplied by means of a four-quadrant amplifier (TREK 10/10B-HS). We used voltages of up to 8 kV, corresponding to a maximum electric field of 160 kV/mm over the total polymer layers thickness, i.e., well below the nominal break-down field of the reference PI material (236 kV/mm).

Driving, control, and data acquisition were performed with a real-time target machine by Speedgoat, running MATLAB Real-time environment. The EBM end-effector stroke was measured via a laser sensor (LK-G152 by Keyence). A protruding structure was attached to the device end effector to facilitate load application and stroke measurement.

Linear muscle testing

Each linear actuation test was performed applying a constant force on the end effector, supplying a time-varying voltage profile on the electrodes, and measuring the resulting displacement. Constant forces at the EBM end effector were generated through a preloaded soft elastic band with an initial length much larger than the actuator stroke. We used sinusoidal voltage profiles, thus reverting the electrode's polarity at each cycle to compensate for polarization of the interfaces between different dielectric layers, as suggested in literature (*24*, *44*). The driving voltage frequency is one-half the resulting actuation frequency. In our results, the percentage contraction (see eq. S15) is defined as the ratio of the stroke and the EBM length before voltage application at the tested load case (average over the performed actuation cycles). The latter is measured from the top surface of the reservoir to the bottom layer surface (where the end effector is attached). The thickness of the end effector is not considered, because its layout is only dictated by experimental convenience, and it can be easily redesigned and optimized.

EBM pump testing

In hydrostatic actuation tests, the EBM fluid outlet was connected to a 3D printed assembly holding custom-made check valves and a membrane bubble. The inflatable membrane was realized using three layers of 500-μm-thick commercial 3M VHB 4905, with a prestretch of about 2.5. In the tests, we preloaded the EBM with a constant force of 1.5 N, and we used sinusoidal voltage inputs with frequency in the range from 1.5 to 3.5 Hz (corresponding to one-half of the resulting actuation frequency). The pressure in the air chamber holding the elastic bubble was measured with pressure sensor MPX12 by Freescale Semiconductor. The bubble volume was estimated via the frames of a high-speed camera (Point Grey GS3-U3-23S6M-C with lens 250F6C). Standard edge detection algorithms were used to resolve the bubble profile, similar to (*41*), and the subtended volume was calculated by numerical integration.

Energy harvester testing

To test the EBM generator, we drove the EBM displacement with linear motor L16-50-35-12-P by Actuonix. The connection between the slider and the EBM end effector was implemented via a fluorocarbon fishing wire (300 μm diameter). Compared with a rigid connection, this ensures a smoother deformation of the EBM and rejects undesired transversal loads, although it does not grant direct drivability of the end-effector position. Similar to actuation tests, the voltage polarity was reverted at any cycle. In the generation tests, we used motor displacements with amplitude of 4 mm, bias of 7.7 mm, and frequency of 0.5 Hz. The input mechanical energy was calculated from the end-effector displacement and the force (measured via a load cell Rb-Phi-118 with RB-Onl-38 amplifier by RobotShop) (see eq. S16). The net generated energy was calculated from the voltage (measured with the amplifier's integrated sensor) and the current (measured with isolation amplifier HCPL-7800A/HCPL-7800 in series to the EBM) (see eq. S16).

SUPPLEMENTARY MATERIALS

robotics.sciencemag.org/cgi/content/full/6/51/eaaz5796/DC1

REFERENCES AND NOTES

1. D. Rus, M. T. Tolley, Design, fabrication and control of soft robots. *Nature* **521**, 467–475 (2015).
2. E. Brown, N. Rodenberg, J. Amend, A. Mozeika, E. Steltz, M. R. Zakin, H. Lipson, H. M. Jaeger, Universal robotic gripper based on the jamming of granular material. *Proc. Natl. Acad. Sci. U.S.A.* **107**, 18809–18814 (2010).
3. B. Mosadegh, P. Polygerinos, C. Keplinger, S. Wennstedt, R. F. Shepherd, U. Gupta, J. Shim, K. Bertoldi, C. J. Walsh, G. M. Whitesides, Pneumatic networks for soft robotics that actuate rapidly. *Adv. Funct. Mater.* **24**, 2163–2170 (2014).
4. M. Wehner, M. T. Tolley, Y. Mengüç, Y.-L. Park, A. Mozeika, Y. Ding, C. Onal, R. F. Shepherd, G. M. Whitesides, R. J. Wood, Pneumatic energy sources for autonomous and wearable soft robotics. *Soft Robot.* **1**, 263–274 (2014).
5. V. Cacucciolo, J. Shintake, Y. Kuwajima, S. Maeda, D. Floreano, H. Shea, Stretchable pumps for soft machines. *Nature* **572**, 516–519 (2019).
6. G. K. Klute, J. M. Czerniecki, B. Hannaford, Artificial muscles: Actuators for biorobotic systems. *Int. J. Rob. Res.* **21**, 295–309 (2002).
7. J. D. W. Madden, N. A. Vandesteeg, P. A. Anquetil, P. G. A. Madden, A. Takshi, R. Z. Pytel, S. R. Lafontaine, P. A. Wieringa, I. W. Hunter, Artificial muscle technology: Physical principles and naval prospects. *IEEE J. Ocean. Eng.* **29**, 706–728 (2004).
8. S. M. Mirvakili, I. W. Hunter, Artificial muscles: Mechanisms, applications, and challenges. *Adv. Mater.* **30**, 1704407 (2018).
9. S. Solano-Arana, F. Klug, H. Mößinger, F. Förster-Zügel, H. F. Schlaak, A novel application of dielectric stack actuators: A pumping micromixer. *Smart Mater. Struct.* **27**, 074008 (2018).
10. A. Jahanshahi, F. Axisa, J. Vanfleteren, Fabrication of an implantable stretchable electro-osmosis pump. *Proc. SPIE* **7929**, 79290R (2011).
11. O. C. Jeong, S. W. Park, S. S. Yang, J. J. Pak, Fabrication of a peristaltic PDMS micropump. *Sens. Actuator. A Phys.* **123-124**, 453–458 (2005).
12. E. Thielicke, E. Obermeier, Microactuators and their technologies. *Mechatronics* **10**, 431–455 (2000).
13. P. Miaudet, A. Derre, M. Maugey, C. Zakri, P. M. Piccione, R. Inoubli, P. Poulin, Shape and temperature memory of nanocomposites with broadened glass transition. *Science* **318**, 1294–1296 (2007).
14. C. S. Haines, M. D. Lima, N. Li, G. M. Spinks, J. Foroughi, J. D. W. Madden, S. H. Kim, S. Fang, M. Jung de Andrade, F. Goktepe, O. Goktepe, S. M. Mirvakili, S. Naficy, X. Lepro, J. Oh, M. E. Kozlov, S. J. Kim, X. Xu, B. J. Swedlove, G. G. Wallace, R. H. Baughman, Artificial muscles from fishing line and sewing thread. *Science.* **343**, 868–872 (2014).
15. Y. Bar-Cohen, Q. Zhang, Electroactive polymer actuators and sensors. *MRS Bull.* **33**, 173–181 (2008).
16. Q. Pei, J. Joseph, R. Kornbluh, R. Pelrine, High-speed electrically actuated elastomers with strain greater than 100%. *Science* **287**, 836–839 (2000).
17. M. Duduta, E. Hajiesmaili, H. Zhao, R. J. Wood, D. R. Clarke, Realizing the potential of dielectric elastomer artificial muscles. *Proc. Natl. Acad. Sci. U.S.A.* **116**, 2476–2481 (2019).
18. G. Kofod, The static actuation of dielectric elastomer actuators: How does pre-stretch improve actuation? *J. Phys. D Appl. Phys.* **41**, 215405 (2008).
19. M. Sadeghi, H. Kim, K. Najafi, Electrostatically driven micro-hydraulic actuator arrays, in *2010 IEEE 23rd International Conference on Micro Electro Mechanical Systems (MEMS)* (IEEE, 2010).
20. H. Kim, K. Najafi, Electrostatic hydraulic three-way gas microvalve for high-pressure applications, in *12th International Conference on Miniaturized Systems for Chemistry and Life Sciences* (MicroTAS, 2008), pp. 369–371.
21. E. Acome, S. K. Mitchell, T. G. Morrissey, M. B. Emmett, C. Benjamin, M. King, M. Radakovitz, C. Keplinger, Hydraulically amplified self-healing electrostatic actuators with muscle-like performance. *Science* **359**, 61–65 (2018).
22. L. Maffli, S. Rosset, H. R. Shea, Zipping dielectric elastomer actuators: Characterization, design and modeling. *Smart Mater. Struct.* **22**, 104013 (2013).
23. M. Duranti, M. Righi, R. Vertechy, M. Fontana, A new class of variable capacitance generators based on the dielectric fluid transducer. *Smart Mater. Struct.* **26**, 115014 (2017).
24. N. Kellaris, V. Gopaluni Venkata, G. M. Smith, S. K. Mitchell, C. Keplinger, Peano-HASEL actuators: Muscle-mimetic, electrohydraulic transducers that linearly contract on activation. *Sci. Robot.* **3**, eaar3276 (2018).
25. M. Taghavi, T. Helps, J. Rossiter, Electro-ribbon actuators and electro-origami robots. *Sci. Robot.* **3**, eaau9795 (2018).
26. R. H. Baughman, Playing nature's game with artificial muscles. *Science* **308**, 63–65 (2005).
27. X. Wang, S. K. Mitchell, E. H. Rumley, P. Rothemund, C. Keplinger, High-strain Peano-HASEL actuators. *Adv. Funct. Mater.* **30**, 1908821 (2019).
28. C. Cao, X. Gao, A. T. Conn, A magnetically coupled dielectric elastomer pump for soft robotics. *Adv. Mater. Technol.* **4**, 1900128 (2019).
29. G. Moretti, M. Duranti, M. Righi, R. Vertechy, M. Fontana, Analysis of dielectric fluid transducers, in *Electroactive Polymer Actuators and Devices (EAPAD) XX* (March 2018), vol. 10594, p. 29, doi: 10.1117/12.2297082.
30. S. J. A. Koh, C. Keplinger, T. Li, S. Bauer, Z. Suo, Dielectric elastomer generators: How much energy can be converted? *IEEE/ASME Trans. Mechatronics* **16**, 33–41 (2011).
31. R. Pelrine, R. D. Kornbluh, J. Eckerle, P. Jeuck, S. Oh, Q. Pei, S. Stanford, Dielectric elastomers: Generator mode fundamentals and applications. *Proc. SPIE 4329, Smart Struct. Mater.* **42**, 148–156 (2001).
32. G. Kovacs, L. Düring, S. Michel, G. Terrasi, Stacked dielectric elastomer actuator for tensile force transmission. *Sens. Actuator. A Phys.* **155**, 299–307 (2009).
33. P. Lotz, M. Matysek, H. F. Schlaak, Fabrication and application of miniaturized dielectric elastomer stack actuators. *IEEE/ASME Trans. Mechatron.* **16**, 58–66 (2011).
34. T. Mirfakhrai, J. D. W. Madden, R. H. Baughman, Polymer artificial muscles. *Mater. Today* **10**, 30–38 (2007).
35. Z. Li, Y. Wang, C. C. Foo, H. Godaba, J. Zhu, C. H. Yap, The mechanism for large-volume fluid pumping via reversible snap-through of dielectric elastomer. *J. Appl. Phys.* **122**, 084503 (2017).
36. P. Linnebach, G. Rizzello, S. Seelecke, Design and validation of a dielectric elastomer membrane actuator driven pneumatic pump. *Smart Mater. Struct.* **29**, 075021 (2020).
37. Y. Chen, L. Agostini, G. Moretti, M. Fontana, R. Vertechy, Dielectric elastomer materials for large-strain actuation and energy harvesting: A comparison between styrenic rubber, natural rubber and acrylic elastomer. *Smart Mater. Struct.* **28**, 114001 (2019).
38. G. Moretti, G. Pietro Rosati Papini, M. Righi, D. Forehand, D. Ingram, R. Vertechy, M. Fontana, Resonant wave energy harvester based on dielectric elastomer generator. *Smart Mater. Struct.* **27**, 035015 (2018).
39. M. Hodgins, A. York, S. Seelecke, Experimental comparison of bias elements for out-of-plane DEAP actuator system. *Smart Mater. Struct.* **22**, 094016 (2013).
40. S. Shian, J. Huang, S. Zhu, D. R. Clarke, Optimizing the electrical energy conversion cycle of dielectric elastomer generators. *Adv. Mater.* **26**, 6617–6621 (2014).
41. R. Kaltseis, C. Keplinger, S. J. A. Koh, R. Baumgartner, Y. F. Goh, W. H. Ng, A. Kogler, A. Tröls, C. C. Foo, Z. Suo, S. Bauer, Natural rubber for sustainable high-power electrical energy generation. *RSC Adv.* **4**, 27905–27913 (2014).
42. I. A. Anderson, I. A. Ieropoulos, T. McKay, B. O'Brien, C. Melhuish, Power for robotic artificial muscles. *IEEE/ASME Trans. Mechatron.* **16**, 107–111 (2011).
43. LINQTAPE ™ PIT1N-Series, *Technical Datasheet* https://caplinq.com/library/technical-data-sheet/#product=175 [accessed 29 January 2020].
44. T. L. Sounart, T. A. Michalske, K. R. Zavadil, Frequency-dependent electrostatic actuation in microfluidic MEMS. *J. Microelectromechanical Syst.* **14**, 125–133 (2005).

Acknowledgments: We thank Nitto Denko Corporation for providing the double-sided adhesive tape used for prototypes manufacturing, CHEROS S.r.l. for providing the PI films used for prototype manufacturing, and F. Damiani for technical support with the experiments. **Funding:** This work was supported by the Italian Ministry of Education, University and Research (MIUR) under the Program Department of Excellence, awarded to the Department of Industrial Engineering of the University of Trento, Italy and to the Scuola Superiore Sant'Anna, Italy. **Author contributions:** M.F. conceived the EBM devices. M.F. and R.V. supervised this research. I.D.S. and G.M. designed the prototypes and carried out the tests. I.D.S., G.M., and G.B. manufactured the prototypes and postprocessed the data. M.B. contributed to the design and construction of the test benches. S.D. and L.F. contributed to materials and manufacturing procedure definition and selection. All the authors contributed to the draft and revised the manuscript. **Competing interests:** The authors declare that they have no competing interests. **Data and materials availability:** All data needed to evaluate the conclusions in the paper are present in the paper or the Supplementary Materials.

Submitted 26 February 2020
Accepted 25 January 2021
Published 24 February 2021
10.1126/scirobotics.aaz5796

Citation: I. D. Sîrbu, G. Moretti, G. Bortolotti, M. Bolignari, S. Diré, L. Fambri, R. Vertechy, M. Fontana, Electrostatic bellow muscle actuators and energy harvesters that stack up. *Sci. Robot.* **6**, eaaz5796 (2021).

Science Robotics

Electrostatic bellow muscle actuators and energy harvesters that stack up

I. D. Sîrbu, G. Moretti, G. Bortolotti, M. Bolignari, S. Diré, L. Fambri, R. Vertechy, and M. Fontana

Sci. Robot. **6** (51), eaaz5796. DOI: 10.1126/scirobotics.aaz5796

Science Robotics (ISSN 2470-9476) is published by the American Association for the Advancement of Science. 1200 New York Avenue NW, Washington, DC 20005. The title *Science Robotics* is a registered trademark of AAAS.